Reliability Engineering and System Safety 213 (2021) 107790

Contents lists available at ScienceDirect

Reliability Engineering and System Safety

journal homepage: www.elsevier.com/locate/ress

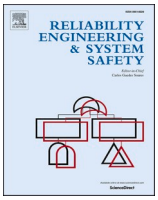

Probabilistic information fusion with point, moment and interval data in reliability assessment

Daoqing Zhou [a], Jingjing He [b], Yi-Mu Du [a], C.P. Sun [a,c,*], Xuefei Guan [a,*]

[a] Graduate School of China Academy of Engineering Physics, Beijing 100193, China
[b] School of Reliability and Systems Engineering, Beihang University, Beijing 100191, China
[c] Beijing Computational Science Research Center, Beijing 100193, China

ARTICLE INFO

Keywords:
Maximum relative entropy
Probabilistic information fusion
Point data
Moment data
Interval data
Hazard rate dynamics

ABSTRACT

This study presents a general framework for probabilistic information fusion with point, moment, and interval data based on the principle of maximum relative entropy. Two types of interval information, namely, the independent interval and the correlated interval, are naturally incorporated in this framework for probability inference. The relative entropy is alternatively expressed using the hazard rate functions associated with the distributions. The probabilistic information fusion problem is recast into a hazard rate dynamics problem, which is solved using Euler-Lagrange method with point, moment, and interval data as boundary conditions. It provides a novel perspective on probabilistic information fusion such that the fusion mechanism is to seek an optimal hazard rate function in the functional space achieving the least action which is expressed as the relative information entropy. The geometry interpretation of the information fusion with point, moment, and interval data, and the effect of processing sequence are signified. An electronic component reliability problem is used to illustrate the basic idea of the method, followed by a fatigue reliability assessment problem demonstrating the overall method. The effectiveness of the method using limited samples and implicit interval information is emphasized using an aeroengine disk lifing application with a risk requirement in airworthiness.

1. Introduction

Probabilistic inference plays an important role in science and engineering applications [1, 2]. The probabilistic inference can in general be divided into forward and inverse problems. The former one deals with uncertainty propagation through existing models given the known and quantitative uncertainty. For example, the estimation of the distribution of response variable given the model and uncertain input variables. The latter one is to assess the model structures and/or estimate unknown parameters given observable data. The inverse problem is much more ubiquitous and the results on models and parameters form the basis of forward predictions. From a practical point of view, probabilistic inference can loosely be seen as a knowledge updating process based on the logical processing of any relevant information. Bayes' theorem provides a rational method to process certain kinds of information for probabilistic inference. The Bayesian methods, in conjunction with the Markov chain Monte Carlo (MCMC) simulations and their variants, have spawned extensive scientific results in almost every disciplines [3–7].

In the field of reliability, the Bayesian method has been widely used to aggregate information to improve the assessment results [8–16]. The basic building blocks of Bayesian methods involve the prior knowledge and observation data, and the two pieces of information interwork through the product rule of conditional probabilities. The construction of the prior distribution in the Bayesian framework has drawn debates over the frequentist and Bayesian. Jaynes proposed formal rules to construct priors, and argued that the maximum entropy principle (MaxEnt) is such a rule [17, 18]. The idea is to construct a probability distribution function that maximizes the information entropy subject to mathematical constraints formed using existing testable information, e.g., statistical moments. The MaxEnt method has been demonstrated in many applications [19–22]. Point observations or measurements are a kind of information that can directly be processed in the Bayesian framework to update the initial prior knowledge. The data are encoded into the likelihood such that the difference between the model prediction and the actual measured one is a random variable following an assumed probability distribution. In the Bayesian framework, there is no formal rule to process statistical moments in updating. This can lead to a certain arbitrariness in processing such

* Corresponding authors.
E-mail addresses: cpsun@csrc.ac.cn (C.P. Sun), xfguan@gscaep.ac.cn (X. Guan).

https://doi.org/10.1016/j.ress.2021.107790
Received 27 November 2020; Received in revised form 10 May 2021; Accepted 12 May 2021
Available online 20 May 2021
0951-8320/© 2021 Elsevier Ltd. All rights reserved.

information. Shore and the collaborators pioneered the method of principle of minimum cross-entropy to estimate the probability distribution using moment data when there exists a prior distribution [23]. It is shown that the cross-entropy, also called the relative entropy, is the only invariant form that satisfies the three axioms of probabilistic inference. To establish a universal and formal rule for both prior construction and probabilistic information fusion, Caticha and Giffin proposed the inference method based on the principle of maximum relative entropy (MrE) [24], allowing for processing both point data and moment data for probability updating. The MrE result reduces to the Bayes' rule when only point data are available, and to the MaxEnt distribution when only moment data are available. The method of MrE has been applied to several problems in different fields including, but not limited to, Refs. [25–29]. In addition, methods based on the evidence theory and related concepts are other alternatives for information fusion [30–32].

Another type of information, given as interval data, is sometimes more widely-seen in the process of design and manufacturing. The boundary or range data may refer the same type of information, depending on the fields of applications. In those cases, the initial design variables are only bounded in some viable ranges based on physical constraints and/or engineering experience. Interval analysis attempts to establish the mapping between the uncertain parameters and the system responses using response surface methods or surrogates [33–37]. It is noted that the interval information can be classified as independent interval and correlated interval. Exploring the variation range of the model response using a combination of the interval endpoints and the sub-divisions can be useful when the uncertain variables are monotonic in the intervals and the response space is smooth [38–42]. Nevertheless, the correlation between uncertain parameters and the non-monotonic variations in the interval cannot be fully incorporated using the classical interval analysis methods. Although the independent interval information is naturally incorporated by changing the integration range of the variables in the method of MrE [43–45], a formal treatment of the correlated interval data is not available in existing methods.

In this study, a probabilistic information fusion framework is formulated based on the principle of MrE, allowing for updating probability using point, moment, and generic interval data. The novelty of the study lies in two aspects. First, the probabilistic information fusion with correlated interval types of data is handled in this framework, which are not systematically dealt with before. Secondly, the relative entropy is alternatively expressed using the hazard rate functions associated with the prior and posterior distributions, and the information fusion problem can be recast to a dynamics problem, which provides a novel perspective on probability inference and a mathematical link to information dynamics. The relative entropy becomes the 'action' that governs the hazard rate dynamics. Resembling the general least-action principle, the hazard rate as the 'velocity' minimizing the 'action' subject to boundary conditions is the most probable hazard rate function. Information such as point, moment, and interval forms the necessary boundary conditions. It is further shown that the independent and correlated intervals resemble the strong and weak boundary conditions, respectively. The remainder of the study is organized as follows. First, the general probabilistic information fusion framework based on the maximum relative entropy is developed to incorporate point, moment, and general interval data. Next, the updating sequence and its effect are discussed in detail. The commutative properties of different types of information are investigated, and the geometry interpretation of the sequence of information fusion is given. Following that, reliability assessment problems are presented to demonstrate the overall method. The influence of the information processing order, as well as the effect of independent and correlated interval data are shown. Finally, conclusions are drawn.

2. Probabilistic information fusion

Consider an uncertain variable $x \in \mathscr{X}$ and some indirect but relevant observable variables $t \in T$. Denote the prior and posterior distributions of x as $p_0(x)$ and $p(x)$ respectively. The probabilistic information fusion is to find an optimal $p(x)$ given $p_0(x)$ and new information relevant to x. The involvement of observable variable t requires the search of the optimal solution in the joint space of $\mathscr{X} \times T$, and the relative entropy of the joint posterior distribution with respect to the joint prior distribution is [23, 24]

$$\boldsymbol{S}(p : p_0) = -\int_{\mathscr{X}\times T} p(x,t)\ln\left[\frac{p(x,t)}{p_0(x,t)}\right]\mathrm{d}x\mathrm{d}t, \tag{1}$$

where $p_0(x,t)$ is the joint prior distribution and $p(x,t)$ is the posterior. The principle of maximum relative entropy states that the optimal posterior is the one that maximizes the entropy term subject to the given constraints. The universal normalization constraint is

$$C_1 : \int_{\mathscr{X}\times T} p(x,t)\mathrm{d}x\mathrm{d}t = 1. \tag{2}$$

The point data, e.g., the measurement value of t, are essentially a constraint on the marginal distribution of t. For a deterministic measurement $t = t'$, the marginal distribution can be expressed as Dirac delta function. In this case, the constraint writes

$$C_2 : \int_{\mathscr{X}\times T} p(x,t)\mathrm{d}x = \delta(t - t'), \tag{3}$$

where $\delta(\cdot)$ is Dirac delta function. The general moment information is often the mean or variance of some test values on x or on a function $f(x)$. Such information can be evaluated as statistical moments and expressed as

$$C_3 : \int_{\mathscr{X}\times T} p(x,t)f(x)\mathrm{d}x\mathrm{d}t = f(x), \tag{4}$$

where $\langle\cdot\rangle$ represents the mathematical expectation. The interval data can be divided into two categories. The first one is the independent interval which limits the bounds of the variable itself. The other one is the correlated interval, which forms the bounds of a function involving two or more variables. Mathematically, the interval data can be expressed as the boundary constraints on variables itself or a general function of two or more variables, such as

$$C_4 : \begin{cases} x \in [x^-, x^+] \\ t \in [t^-, t^+] \\ q(x,t) \in [q^-, q^+] \end{cases}, \tag{5}$$

where $q(x,t)$ represents a general function involving two variables x and t in this case. The format of this function determines how the participating variables interact with each other.

To maximize the relative entropy of Eq. (1) based on the given information in terms of constraints C_1-C_4, the variational term is required

$$\delta\Lambda = \delta\left(-\int_{\mathscr{X}\times T} p(x,t)\left\{\ln\left[\frac{p(x,t)}{p_0(x,t)}\right] - \alpha - \beta f(x) - \lambda(t)\right\}\mathrm{d}x\mathrm{d}t\right) = 0, \tag{6}$$

where α, β, and $\lambda(t)$ are Lagrange multipliers to be determined. To view the solution to Eq. (6) from a dynamical perspective, the following formulation of probabilistic information fusion using hazard rate dynamics is proposed.

2.1. Formulation of probabilistic information fusion using hazard rate dynamics

The relative entropy as the action of the joint hazard rate dynamics is formulated in this section. Denote the joint cumulative density function (CDF) of x and t as $F(x,t)$ such that

$$F(x,t) = \Pr(X < x, T < t) = \int_{\tilde{x}<x,\tilde{t}<t} p(\tilde{x},\tilde{t})\mathrm{d}\tilde{x}\mathrm{d}\tilde{t} \tag{7}$$

and $R(x,t)$ is the survival function which relates to the CDF by

$$R(x,t) = 1 - F(x,t). \tag{8}$$

The joint probability density function (PDF) of the optimal posterior can be more generally expressed using the CDF or its associated survival function.

$$p(x,t) \equiv \partial_x\partial_t[F(x,t)] = -\partial_x\partial_t[R(x,t)], \tag{9}$$

where $\partial_x\partial_t[\cdot]$ represents the double differentiation operator. The joint hazard rate function by definition is

$$h(x,t) = -\frac{\partial_x\partial_t[R(x,t)]}{R(x,t)}. \tag{10}$$

Integration of Eq. (10) on both sides to have,

$$R(x,t) = \exp\left[-\int_{\tilde{x}<x,\tilde{t}<t} h(\tilde{x},\tilde{t})\mathrm{d}\tilde{x}\mathrm{d}\tilde{t}\right]. \tag{11}$$

Denote

$$Y(x,t) = \int_{\tilde{x}<x,\tilde{t}<t} h(\tilde{x},\tilde{t})\mathrm{d}\tilde{x}\mathrm{d}\tilde{t}. \tag{12}$$

The survival function can be written as

$$R(x,t) = \exp[-Y(x,t)], \tag{13}$$

and the PDF can be expressed using the functional $Y(x,t)$ by Eq. (9) as

$$p(x,t) = -\partial_x\partial_t\{\exp[-Y(x,t)]\} = (\partial_x\partial_t Y - \partial_x Y\partial_t Y)\exp[-Y(x,t)]. \tag{14}$$

Denote the Lagrangian term in Eq. (6) as

$$\mathscr{L} = -p(x,t)\left\{\ln\left[\frac{p(x,t)}{p_0(x,t)}\right] - g(x,t)\right\}, \tag{15}$$

where

$$g(x,t) = -\alpha - \beta f(x) - \lambda(t). \tag{16}$$

To minimize the 'action', i.e., the relative entropy, Y satisfies the Euler-Lagrange equation

$$\begin{aligned}\delta\Lambda[Y(x,t)] &= \delta\left[\int_{\mathscr{X}\times T}\mathscr{L}(Y,\partial_x Y,\partial_t Y,\partial_x\partial_t Y)\mathrm{d}x\mathrm{d}t\right]\\ &= \delta\int_{\mathscr{X}\times T}\left[\frac{\partial\mathscr{L}}{\partial Y} - \sum_i\partial_i\frac{\partial\mathscr{L}}{\partial[\partial_i Y]} + \partial_x\partial_t\frac{\partial\mathscr{L}}{\partial[\partial_x\partial_t Y]}\right]\delta Y\mathrm{d}x\mathrm{d}t\end{aligned} \tag{17}$$

where $\partial_i[\cdot]$ is the partial derivative with respect to the variable $i \in (x,t)$. Therefore, the equation of motion writes

$$\frac{\partial\mathscr{L}}{\partial Y} - \sum_i\partial_i\frac{\partial\mathscr{L}}{\partial[\partial_i Y]} + \partial_x\partial_t\frac{\partial\mathscr{L}}{\partial[\partial_x\partial_t Y]} = 0. \tag{18}$$

The general solution to Eq. (18) is found as, following the steps shown in Appendix,

$$\ln\frac{p(x,t)}{p_0(x,t)} = -a(x) - b(t) - c. \tag{19}$$

For independent interval, i.e., the bounds of the variable itself, the variation requires the boundary values of the function and the first order partial derivative remain constants. This condition can be expressed as

$$\begin{cases}\ln\dfrac{p(x,t^{\pm})}{p_0(x,t^{\pm})} = g(x,t^{\pm})\\ \ln\dfrac{p(x^{\pm},t)}{p_0(x^{\pm},t)} = g(x^{\pm},t)\\ \partial_x\ln\dfrac{p(x,t^{\pm})}{p_0(x,t^{\pm})} = \partial_x g(x,t^{\pm})\\ \partial_t\ln\dfrac{p(x^{\pm},t)}{p_0(x^{\pm},t)} = \partial_t g(x^{\pm},t)\end{cases}, \tag{20}$$

where the superscript '$^{\pm}$' represents the possible bounds. The terms $a(x)$, $b(t)$, and c that satisfy the boundary condition are

$$\begin{cases}a(x) = \beta f(x)\\ b(t) = \lambda(t)\\ c = \alpha\end{cases}. \tag{21}$$

Therefore, the Eq. (19) can be rewritten as

$$\ln\frac{p(x,t)}{p_0(x,t)} = -\alpha - \beta f(x) - \lambda(t). \tag{22}$$

Finally, the optimal posterior PDF is determined as

$$p(x,t) = p_0(x,t)\exp[-\alpha - \beta f(x) - \lambda(t)]. \tag{23}$$

The multiplier α is some unknown constant, Eq. (23) can further be expressed as

$$p(x,t) = p_0(x,t)\exp[-\beta f(x) - \lambda(t)]/Z', \tag{24}$$

where

$$Z' = \int_{\mathscr{X}\times T} p_0(x,t)\exp[-\beta f(x) - \lambda(t)]\mathrm{d}x\mathrm{d}t \tag{25}$$

is the normalizing constant. Substitute $p(x,t)$ in Eq. (3) and Eq. (1) with Eq. (24) to obtain

$$p(x,t) = \frac{p_0(x,t)\delta(t-t')\mathrm{e}^{-\beta f(x)}}{\int_{\mathscr{X}} p_0(x,t)\mathrm{e}^{-\beta f(x)}\mathrm{d}x}. \tag{26}$$

Integrating over the observable t yields

$$p(x) = \frac{p_0(x)p_0(t'|x)\mathrm{e}^{-\beta f(x)}}{Z}, \tag{27}$$

where

$$Z = \int_x p_0(x)p_0(t'|x)\mathrm{e}^{-\beta f(x)}\mathrm{d}x \tag{28}$$

is the normalizing constant, and the Lagrange multiplier β is obtained by $\partial\ln Z/\partial(-\beta) = \langle f(x)\rangle$.

2.2. Points data

With the point data only and no moment nor interval data, the constraint set $\boldsymbol{C} = \{C_1, C_2, C_3, C_4\}$ is reduced to the normalization constraint C_1 and point data C_2. The corresponding equation $g(x,t)$ in Eq. (16) reduces to

$$g(x,t) = -\alpha - \lambda(t). \tag{29}$$

The general solution in this case is

$$\ln\frac{p(x,t)}{p_0(x,t)} = -b(t) - c \tag{30}$$

and

$$\begin{cases}b(t) = \lambda(t)\\ c = \alpha\end{cases}. \tag{31}$$

The optimal posterior distribution only with the point observation is indicated as

$$p(x) = p_0(x)p_0(t'|x)/Z_p, \tag{32}$$

where $Z_p = \int^{p_0}(x)p_0(t'|x)\mathrm{d}x$ is normalizing constant. This result reproduces the classical Bayesian posterior with a single point observable t'. For a set of independent observables $\boldsymbol{t}' = (t_1', t_2', \ldots, t_n')$, the optimal posterior, following the same process, is

$$p(x) = p_0(x)p(\boldsymbol{t}'|x) \Big/ Z_{\boldsymbol{p}} = p_0(x)\prod_{i=1}^{n} p_0(t_i'|x) \Big/ Z_{\boldsymbol{p}}, \tag{33}$$

where $Z_{\boldsymbol{p}} = \int^{p_0}(x)p_0(\boldsymbol{t}'x)\mathrm{d}x$. The result of multiple observables also reproduces a Bayesian posterior.

2.3. Moment data

With only the moment constraint C_3 and the universal normalization constraint C_1, the term $g(x,t)$ in Eq. (16) reduces to

$$g(x,t) = -\alpha - \beta f(x). \tag{34}$$

The general solution in this case is

$$\ln\frac{p(x,t)}{p_0(x,t)} = -a(x) - c \tag{35}$$

and

$$\begin{cases} a(x) = \beta f(x) \\ c = \alpha \end{cases}. \tag{36}$$

The resulting optimal posterior PDF is obtained as

$$p(x) = p_0(x)\mathrm{e}^{-\beta f(x)}/Z_m, \tag{37}$$

where $Z_m = \int^{p_0}(x)\mathrm{e}^{-\beta f(x)}\mathrm{d}x$ is the normalizing constant, and β is obtained by resolving the equation $\partial \ln Z_m/\partial(-\beta) = \langle f(x)\rangle$. Eq. (37) reproduces the MaxEnt PDF when only moment data are given.

Given a set of general functions, for example, $\boldsymbol{f}(x) = \{f_1(x), f_2(x), \ldots, f_k(x)\}$, and its corresponding moment set $\langle \boldsymbol{f}(x)\rangle = \{\langle f_1(x)\rangle, \langle f_2(x)\rangle, \ldots, \langle f_k(x)\rangle\}$, the updated posterior is found to be

$$p(x) = p_0(x)\exp\left[-\sum_{i}^{k}\beta_i f_i(x)\right] \Big/ Z_{\boldsymbol{m}}, \tag{38}$$

where $Z_{\boldsymbol{m}} = \int^{p_0}(x)\exp[-\sum_i^m \beta_i f_i(x)]\mathrm{d}x$ is the corresponding normalizing constant. Note that Eq. (38) is identical to the MaxEnt PDF when multiple moment data constraints are used.

2.4. Interval data

The interval data are implicitly encoded in the updating process as the integral bounds, and can be divided into two categories, namely, the independent and correlated intervals. The former one resembles a 'strong' boundary condition in many differential and integral problems as it directly limits the variable itself. The latter one resembles a 'weak' boundary condition, and it sets up bounds for the hypersurface formed by the participating variables through the function $q(x,t)$ in Eq. (5). For example, $q(x,t) = x{\cdot}t$ and $q^- \le x{\cdot}t \le q^+$. The two kinds of interval data are discussed below.

2.4.1. Independent interval

Independent interval data refer to the direct limits on the variables itself or its functions. Using the previous notations, the range of the parameter $x \in [x^-, x^+]$ solely limits the values of x. The corresponding constraint sets the integration domain in the normalizing constant.

$$Z = \int_{x^-}^{x^+} p_0(x)p_0(t'|x)\mathrm{e}^{-\beta f(x)}\mathrm{d}x. \tag{39}$$

In this simple case where only a direct interval constraint is imposed on the variable x and no other imposed constraint such as moment and point data, the components of $p_0(t'x)$ and $e^{-\beta f(x)}$ in Eqs. (27)-(28) are dropped off from the two equations. In this case, only the integration range changes according to the interval limits, and it yields the truncated version of the prior PDF. This case is later demonstrated by Case 3 in Section 4.1.

In addition, the range of an invertible function of x can also be used to resolve the limits on x. Without loss of generality, consider a single-variable invertible function $y = \mathscr{Y}(x) \in [y^-, y^+]$. The range limits on $\mathscr{Y}(x)$ can be converted to the range limits on x using the inverse $x = \mathscr{Y}^{-1}(y), y \in [y^-, y^+]$. In this case, the integration range can be expressed as $x \in \{\mathscr{Y}^{-1}(y)\}$, s.t. $y^- \le y \le y^+$, and the normalizing constant is

$$Z = \int_{x\in\left\{\mathscr{Y}^{-1}(y)\right\},\ \text{s.t. } y^-\le y\le y^+} p_0(x)p_0(t'|x)\mathrm{e}^{-\beta f(x)}\mathrm{d}x. \tag{40}$$

Given that the function $\mathscr{Y}(x)$ is monotonic increasing or decreasing, the range of x can be simplified to $x \in [\mathscr{Y}^{-1}(y^-), \mathscr{Y}^{-1}(y^+)]$ or $x \in [\mathscr{Y}^{-1}(y^+), \mathscr{Y}^{-1}(y^-)]$, respectively. It is worth mentioning that the range of t does not have a non-trivial effect as the integration involving the Dirac delta function returns a constant regardless of range of the variable, as can be seen from Eq. (26). In this case, the range of t does not change the result of Eq. (27). The use of Direct delta indicates that the observation itself is precise.

2.4.2. Correlated interval

Correlated interval refers to the cases where the range of a multivariate scaler function involving two or more variables is bounded. The ranges of individual variables depend on each other. Denote a k-dimensional parameter as $\mathbf{x} = (x_1, x_2, \ldots, x_k)$ and the scaler function as $y = \mathscr{Y}(\mathbf{x}) \in [y^-, y^+]$. The general expression for the normalizing constant is

$$Z = \int_{\mathbf{x}\in\mathscr{Y}^{-1}(y)\text{s.t.}y^-\le y\le y^+} p_0(\mathbf{x})p_0(t'|\mathbf{x})\mathrm{e}^{-\beta f(\mathbf{x})}\mathrm{d}\mathbf{x}. \tag{41}$$

For instance, a bivariate function $\mathscr{Y}(\mathbf{x}) = x_1{\cdot}x_2$ bounded in the range of $[-1, 1]$ with x_1 and x_2 spanning the entire real domain. In this case, the valid ranges of x_1 and x_2 depend on each other, as illustrated in Fig. 1. It is also possible that the resulting region is a union of several isolated subregions.

Despite the normalizing constant can be difficult to evaluate, particularly, for the case of correlated interval, knowing the constant is not necessarily needed in practical problems when sampling-based methods are used. Sampling in conjunction with an accept-rejection scheme such as Metropolis-Hastings and its variants allows for drawing samples from unnormalized distributions [46]. To resolve β, the Monte Carlo (MC)-based numerical integration can be made at a set of test values of β, see, e.g., simulated tempering technique in Chap. 12.4 of Ref. [47]. It is also viable to approximate this normalizing constant using asymptotic approximations such as Laplace approximations [48–50] for high-dimensional problems or standard quadrature rules for low-dimensional problems. The determination of the proper numerical technique in resolving the value of β in high-dimensional problem is beyond the goal and scope of this study and can be found elsewhere.

To summarize, the equations for each type of data are listed in Table 1. The effect of information fusion order on updating results is discussed next.

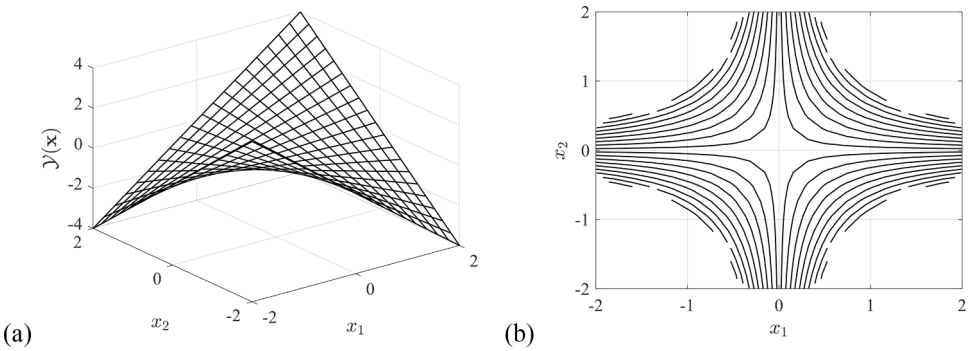

Fig. 1.. Illustration of the interval data bounded by a function of $\mathscr{Y}(\mathbf{x}) = x_1 \cdot x_2$. (a) The surface of $\mathscr{Y}(\mathbf{x})$, and (b) the valid region of (x_1, x_2) by $-1 \le \mathscr{Y}(\mathbf{x}) \le 1$, shown as the area enveloped by the quadratic perimeters. Note x_1 and x_2 are not limited to $[-2, 2]$.

Table 1.
The summary table with the posterior distribution updated by different information types.

Information type	The posterior distribution	The normalization function
Point data	$p(x) = p_0(x)p_0(t'\|x)/Z_p$	$Z_p = \int^{p_0}(x)p_0(t'x)\mathrm{d}x$
Moment data	$p(x) = p_0(x)\mathrm{e}^{-\beta_m f(x)}/Z_m$	$Z_m = \int^{p_0}(x)\mathrm{e}^{-\beta_m f(x)}\mathrm{d}x$
Moment and interval data	$p(x) = p_0(x)\mathrm{e}^{-\beta_i f(x)}/Z_i$	$Z_i = \int_{\mathscr{I}} p_0(x)\mathrm{e}^{-\beta_i f(x)}\mathrm{d}x$
Point, moment and interval data	$p(x) = p_0(x)p_0(t'\|x)$ $\mathrm{e}^{-\beta f(x)}/Z$	$Z = \int_{\mathscr{I}} p_0(x)p_0(t'\|x)\mathrm{e}^{-\beta f(x)}\mathrm{d}x$

3. Dependence of information fusion sequence

It is noted that different results are obtained when information is processed in different order sequentially or simultaneously. It may appear as an inconsistency of the method; however, as Jaynes argued in the method of MaxEnt, the difference is not due to the method but due to the way how these pieces of information are used. The argument can further be strengthened using the concept of hazard rate dynamics presented in Section 2.1. The mechanism of the proposed probabilistic information fusion framework allows for the interpretation of the sequence effect. Different ways in information processing are just different boundary conditions set by the practitioner (not the method itself) when the least action of the hazard rate dynamics is sought.

3.1. Order of information fusion

The influence of the order of information processing can be inspected by applying the point, moment, and interval constraints sequentially and simultaneously. As previously mentioned, the interval constraint implicitly affects the result through the normalizing constant, and the interval constraint of point observation has no effect due to the use of Dirac delta function. Therefore, the interval constraint on uncertain variable x makes the result different.

3.1.1. Simultaneous fusion with point, moment, and interval

The application of the point, moment, and interval constraints reproduces the optimal posterior PDF in Eq. (27) and the corresponding normalizing constant in Eq. (28). In particular, the normalizing constant is obtained by integration over the domain consistent with the interval constraint.

$$p_1(x) = \frac{p_0(x)p(t'|x)\mathrm{e}^{-\beta_1 f(x)}}{\int_{\mathscr{D}_1} p_0(x)p(t'|x)\mathrm{e}^{-\beta_1 f(x)}\mathrm{d}x} = \frac{p_0(x)p(t'|x)\mathrm{e}^{-\beta_1 f(x)}}{Z_1}, \tag{42}$$

where $Z_1 = \int_{\mathscr{D}_1} p_t(x)\mathrm{e}^{-\beta_1 f(x)}\mathrm{d}x$ and β_1 is determined by the equation $\partial \ln Z_1/\partial(-\beta_1) = \langle f(x)\rangle$, and the domain $\mathscr{D}_1$ represents the valid range of x based on the interval constraint.

3.1.2. Sequential fusion of point, moment, and interval

The initial result of the posterior PDF with point data is

$$p_t(x) = \frac{p_0(x)p(t'|x)}{\int_{\mathscr{D}_t} p_0(x)p(t'|x)\mathrm{d}x} = \frac{p_0(x)p(t'|x)}{Z_t}, \tag{43}$$

where the normalizing constant $Z_t = \int_{\mathscr{D}_t} p_0(x)p(t'|x)\mathrm{d}x$. The continuous updating with moment constraint using the point updated one can be found as

$$p_{2,m}(x) = \frac{p_t(x)\mathrm{e}^{-\beta_2 f(x)}}{\int_{\mathscr{D}_{2,m}} p_t(x)\mathrm{e}^{-\beta_2 f(x)}\mathrm{d}x} = \frac{p_0(x)p(t'|x)\mathrm{e}^{-\beta_2 f(x)}}{Z_{2,m}}, \tag{44}$$

where $Z_{2,m} = \int_{\mathscr{D}_{2,m}} p_t(x)\mathrm{e}^{-\beta_2 f(x)}\mathrm{d}x$ and β_2 is obtained by the equation $\partial \ln Z_{2,m}/\partial(-\beta_2) = \langle f(x)\rangle$. Finally, the interval constraint, if is independent and different from the domain $\mathscr{D}_{2,m}$ associated with the moment constraint, can yield a truncated version of $p_{2,m}(x)$. Due to a different domain $\mathscr{D}_2$ produced by this interval data, updating $p_{2,m}(x)$ with the domain $\mathscr{D}_2$ yields the optimal posterior as

$$p_2(x) = \frac{p_0(x)p(t'|x)\mathrm{e}^{-\beta_2 f(x)}}{Z_2}, \tag{45}$$

where $Z_2 = \int_{\mathscr{D}_2} p_0(x)p(t'|x)\mathrm{e}^{-\beta_2 f(x)}\mathrm{d}x$. Note that $Z_2 \neq Z_{2,m}$ and β_2 is solved by $Z_{2,m}$, not Z_2.

3.1.3. Sequential fusion of point, and moment with interval

This case is different from the previous one as the interval data are applied with the moment data simultaneously. The initial point updated result is identical to Eq. (43), and the result after applying the moment and interval constraints together is

$$p_3(x) = \frac{p_t(x)\mathrm{e}^{-\beta_3 f(x)}}{\int_{\mathscr{D}_3} p_t(x)\mathrm{e}^{-\beta_3 f(x)}\mathrm{d}x} = \frac{p_0(x)p(t'|x)\mathrm{e}^{-\beta_3 f(x)}}{Z_3}, \tag{46}$$

where $Z_3 = \int_{\mathscr{D}_3} p_t(x)\mathrm{e}^{-\beta_3 f(x)}\mathrm{d}x$ and β_3 is solved by $\partial \ln Z_3/\partial(-\beta_3) = \langle f(x)\rangle$.

3.1.4. Sequential fusion of moment, interval, and point

The initial moment updated posterior is

$$p_{4,m}(x) = \frac{p_0(x)\mathrm{e}^{-\beta_4 f(x)}}{\int_{\mathscr{D}_{4,m}} p_0(x)\mathrm{e}^{-\beta_4 f(x)}\mathrm{d}x} = \frac{p_0(x)\mathrm{e}^{-\beta_4 f(x)}}{Z_{4,m}}, \tag{47}$$

where $Z_{4,m} = \int_{\mathscr{D}_{4,m}} p_0(x)\mathrm{e}^{-\beta_4 f(x)}\mathrm{d}x$ and β_4 is determined by the equation $\partial \ln Z_{4,m}/\partial(-\beta_4) = \langle f(x)\rangle$. Next, the imposing of the interval constraint forms a truncated version of Eq. (47) if the resulting domain is different from domain $\mathscr{D}_{4,m}$. Denote this domain as $\mathscr{D}_4$ and note that $\mathscr{D}_4 \neq \mathscr{D}_{4,m}$. The updated posterior is

$$p_4(x) = \frac{p_0(x)\mathrm{e}^{-\beta_4 f(x)}}{\int_{\mathscr{D}_4} p_0(x)\mathrm{e}^{-\beta_4 f(x)}\mathrm{d}x} = \frac{p_0(x)\mathrm{e}^{-\beta_4 f(x)}}{Z_4}, \tag{48}$$

where $Z_4 = \int_{\mathscr{D}_4} p_0(x)\mathrm{e}^{-\beta_4 f(x)}\mathrm{d}x$, which is different from $Z_{4,m}$. Note that β_4 is obtained using $Z_{4,m}$ not Z_4. The updated PDF with the point observation is obtained by using Eq. (48) as the prior, as

$p_{4,t}(x) = \frac{p_0(x)p_0(t'|x)\mathrm{e}^{-\beta_4 f(x)}}{\int_{\mathscr{D}_4} p_0(x)p_0(t'|x)\mathrm{e}^{-\beta_4 f(x)}\mathrm{d}x} = \frac{p_0(x)p_0(t'|x)\mathrm{e}^{-\beta_4 f(x)}}{Z_{4,t}}$, (49) where $Z_{4,t} = \int_{\mathscr{D}_4} p_0(x)p_0(t'|x)\mathrm{e}^{-\beta_4 f(x)}\mathrm{d}x$.

3.1.5. Sequential fusion of moment with interval, and point

Updating using moment with interval yields the following posterior PDF

$$p_5(x) = \frac{p_0(x)\mathrm{e}^{-\beta_5 f(x)}}{\int_{\mathscr{D}_5} p_0(x)\mathrm{e}^{-\beta_5 f(x)}\mathrm{d}x} = \frac{p_0(x)\mathrm{e}^{-\beta_5 f(x)}}{Z_5}, \tag{50}$$

where $Z_5 = \int_{\mathscr{D}_5} p_0(x)\mathrm{e}^{-\beta_5 f(x)}\mathrm{d}x$ is the normalizing constant and β_5 is resolved using $\partial \ln Z_5/\partial(-\beta_5) = \langle f(x)\rangle$. Note the interval data are encoded in the resulting integration domain $\mathscr{D}_5$. Use Eq. (50) as the prior and perform updating with the point data, the final posterior PDF is

$$p_{5,t}(x) = \frac{p_0(x)p_0(t'|x)\mathrm{e}^{-\beta_5 f(x)}}{\int_{\mathscr{D}_5} p_0(x)p_0(t'|x)\mathrm{e}^{-\beta_5 f(x)}\mathrm{d}x} = \frac{p_0(x)p_0(t'|x)\mathrm{e}^{-\beta_5 f(x)}}{Z_{5,t}}, \tag{51}$$

where $Z_{5,t} = \int_{\mathscr{D}_5} p_0(x)p_0(t'|x)\mathrm{e}^{-\beta_5 f(x)}\mathrm{d}x$.

There are trivial cases such as processing point data with interval, prior to or after the moment data; however, as mentioned previously the interval constraints make no difference on the point data due to the Dirac delta function which represents a precise observation itself, the results of these cases are reduced to those discussed ones.

3.2. Commutative property of different types of information

The probabilistic information fusion results in Eqs. (27) and (33) indicate that the point data used separately or simultaneously produce the same results. This is consistent with the Bayesian method as the point data are fused through the likelihood function, following the product rule of probability. Therefore, multiple points are interchangeable, and they are commutative in the information fusion process. Note that the measurements are independent in nature; consequently, the joint inference space is $\Omega = X \times \boldsymbol{T}$, where the space $\boldsymbol{T} = T_1 \times T_2 \times, \ldots, \times T_n$. The term $T_i, i \in (1, 2, \ldots, n)$ is the state space of the point t_i. This can be understood as the space T_i 'collapses' to a singular t_i after integrating the Dirac term in Eq. (26). Therefore, the updating process resembles the collapse of an n-dimensional space $\boldsymbol{T}$ to an n-dimensional point $\boldsymbol{t} = (t_1, t_2, \ldots, t_n)$. The order is irrelevant as the final location is prescribed, making the point data commutative. It also shows that the interval constraints make no effect on point data as the point $\boldsymbol{t}$ has no volume in the space of $\boldsymbol{T}$. As shown in Fig. 2 (a), as long as the available point data $\boldsymbol{t} = (t_1, t_2, t_3)$ are used, the joint space 'collapses' to the point $\boldsymbol{t}$, irrelevant to the order. The shades illustrate the possible values of t_2. The commutative nature of point data is later demonstrated in Section 4.1 where Case 4 and Case 6 have identical results.

The moment data and the resulting constraints $\int_X p(x,t) f_i(x)\mathrm{d}x = \langle f_i(x)\rangle, i \in (1, 2, \ldots, k)$ are associated with the space of X. Therefore, the moment data fusion process can be considered as a 'tuning' of the parameter β_i in meeting the constraint, and the moment data are noncommutative. When the interval data are fused in conjunction with the moment data, the interval data also become noncommutative.

The cases related to order of information processing mentioned in Section 3.1 are further elucidated by the geometry illustration shown in Fig. 2(b). The planes satisfying the point, moment and interval constraints are represented by C_2, C_3 and C_4 respectively, which corresponds to the constraint expression in Section 2.1. The $p_i,\ i \in (1,\ 2, \ldots,\ 5)$ corresponds to the different order of information processing analyzed in Section 3.1. The point constraint is applied to information processing by multiplying the probability and likelihood function (just like p_t, $p_{4,t}$ and $p_{5,t}$), therefore the order of point data processing is commutative and multiple point data do not affect each other. The moment constraint is to make the result satisfy the known constraint by adjusting the β value, which is influenced by the integrand function of the normalized parameter. Compared with the p_3 and p_5, due to the different processing order leads to the different integrand function and value of β, the update result is obviously different, which is illustrated that the moment information is noncommutative.

4. Engineering applications

A reliability problem of electronic components is presented to demonstrate the overall method using point, moment, and interval data. The influence of fusion sequence on the result is shown. Following this, a practical fatigue problem involving joint interval data is presented in detail. A realistic aeroengine disk lifing with risk requirement in airworthiness furthers shows the significance of the proposed method in making an effective assessment by fusing the implicit interval data. The value of β in the posterior PDFs in the examples are resolved using numerical methods in Octave or MATLAB by solving the equation of $\partial \ln Z/\partial(-\beta) = \langle f(x)\rangle$ with the *fsolve* (built-in) function and the numerical derivative scheme *derivest*.[1] The normalizing constant Z is evaluated using the (built-in) integration functions *integral/quadgk/quad2d*.

4.1. Reliability of an electrical component

Assume the life of an electrical component, t, follows an extreme value distribution with a parameter of x, and the life distribution conditional on a given x can be expressed as $p_0(tx) = \mathrm{e}^{t-x-\mathrm{e}^{t-x}}$. In addition, the parameter x follows a simplified Weibull prior distribution of $p_0(x) = \mathrm{e}^{-x}$ for $x > 0$. In this case, the joint prior distribution can be expressed as

$$p_0(x,t) = p_0(x)p_0(tx) = \mathrm{e}^{t-2x-\mathrm{e}^{t-x}}. \tag{52}$$

The statistical moment data, $\langle f(x)\rangle = 0.6$, are acquired from one manufacturing factory. A series of life testing results $\boldsymbol{t}' = (t_1', t_2', t_3') = (1,\ 1.3,\ 0.9)$ (in years) are obtained at the consumer side. In addition, it is found that based on the survey of all the manufacturing factories, the control parameter x falls in the range of $[0,\ 2]$. Given above information, one would like to know the revised reliability of this component continuously working for at least three months, i.e., $\Pr(t > 0.25)$. It can be seen that the final result depends on how those pieces of information are fused, which in turn are associated with the questions being asked.

The PDFs obtained using different information processing schemes are presented in Table 2, where Cases 1–3 are results updated with point, moment, and interval data only, respectively, and Cases 4–8 are results obtained with the orders described in Sections 3.1.1–3.1.5, respectively. The corresponding reliability,

$$R|_{t=0.25} = \Pr(t > 0.25) \tag{53}$$

are obtained using the resulting PDFs and given in the last column of the table. Fig. 3 presents the reliability curves associated with different results, where the large deviations appear in the tail region of the curves. It is worth stressing that different PDFs can be obtained when the same amount of information is processed differently, and there is no universal rule to guide how information should be processed.

It is worth noting that the point data are incorporated through the likelihood function, following the product rule of probability. The

[1] D'Errico, J. (2021). Adaptive Robust Numerical Differentiation (https://www.mathworks.com/matlabcentral/fileexchange/13490-adaptive-robust-numerical-differentiation), MATLAB Central File Exchange.

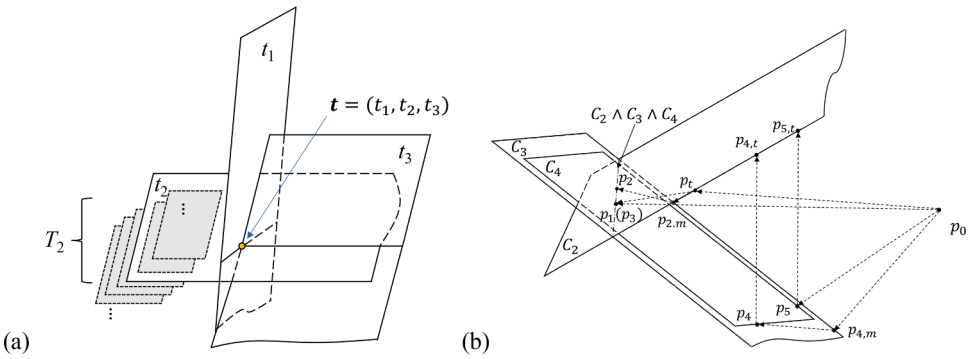

Fig. 2.. (a) Illustration of the commutative property of point data in probabilistic information fusion, and (b) the geometry illustration of information fusion with multiple constraints.

Table 2.
Posterior PDFs obtained using different information fusion schemes. Cases 1–3 are results obtained only with point, moment, and interval data, respectively. Cases 4–8 are results obtained according to the schemes described in Sections 3.1.1-3.1.5 respectively.

Case	The posterior distribution	β	Reliability
1	$p_1(x) = 44.1465e^{3.2-4x-e^{1-x}-e^{1.3-x}-e^{0.9-x}}$	N/A	0.8944
2	$p_2(x) = 1.6667e^{-1.6667x}$	0.6667	0.8557
3	$p_3(x) = 1.1565e^{-x}$ for $x \in [0,\ 2]$	N/A	0.8682
4	$p_4(x) = 159.72e^{3.2-5.7331x-e^{1-x}-e^{1.3-x}-e^{0.9-x}}$	1.7331	0.8574
5	$p_5(x) = 162.45e^{3.2-5.7613x-e^{1-x}-e^{1.3-x}-e^{0.9-x}}$	1.7613	0.8569
6	$p_6(x) = 159.72e^{3.2-5.7331x-e^{1-x}-e^{1.3-x}-e^{0.9-x}}$	1.7331	0.8574
7	$p_7(x) = 77.0945e^{3.2-4.6667x-e^{1-x}-e^{1.3-x}-e^{0.9-x}}$	0.6667	0.8776
8	$p_8(x) = 59.0957e^{3.2-4.3360x-e^{1-x}-e^{1.3-x}-e^{0.9-x}}$	0.3360	0.8841

moment data fusion process satisfies the constraint by adjusting the value of β. Therefore, the order of point information is commutative, and updated results with moment constraints depend on the value of β. Due to the same normalization functions Z_1 and Z_3, the values of β_1 and β_3 are determined to be the same by resolving the equation $\partial \ln Z / \partial(-\beta) = \langle f(x) \rangle$. Therefore, the different orders of information fusion in Case 4 and Case 6 lead to the same posterior distribution.

The example demonstrates probabilistic information fusion with three types of data, namely, the point, moment, and interval data. The sequence of information fusion and its influence on the results are signified. Next, a realistic engineering application example is presented to further demonstrate the probabilistic information fusion with correlated interval data and its impact to the fatigue reliability assessment.

4.2. Probabilistic fatigue life prediction and reliability assessment

A fatigue crack growth problem is adopted here to demonstrate the overall method in realistic problems. Point, moment, and correlated interval data are used for probabilistic information fusion, results are compared to illustrate the influence of different information on life prediction results.

4.2.1. Fatigue crack growth life prediction model and prior PDF of parameters

To demonstrate the correlated interval, a strain energy density factor-based fatigue crack growth model is employed to describe the fatigue crack growth rate under a cyclic loading condition [51],

$$\mathrm{d}a/\mathrm{d}N = B(\Delta S)^n, \tag{54}$$

where a is the crack length, N is the number of load cycles, $\mathrm{d}a/\mathrm{d}N$ is the crack growth rate per one load cycle, ΔS is the variation of the strain energy density factor in one cycle, and B and n are fitting parameters. The strain energy density factor relates to the mixed mode stress intensity factors through two correlated material parameters, namely, the shear modulus G and Poisson's ratio ν, allowing for mixed mode fatigue crack growth prediction [52],

$$S = a_{11}\cdot {K_1}^2 + 2\cdot a_{12}\cdot K_1 \cdot K_2 + a_{22}\cdot {K_2}^2 + a_{33}\cdot {K_3}^2, \tag{55}$$

where K_1, K_2, and K_3 are stress intensity factors of modes I, II, and III, respectively, and a_{ij} are coefficients involving the shear modulus G and Poisson's ratio ν, and are $a_{11} = (3 - 4\nu - \cos\theta)(1 + \cos\theta)/(16G)$, $a_{12} = (2\sin\theta)[\cos\theta - (1 - 2\nu)]/(16G)$, $a_{22} = [4(1 - \nu)(1 - \cos\theta) + (1 + \cos\theta)(3\cos\theta - 1)]/(16G)$, and $a_{33} = 1/(4G)$, respectively. The term θ is the angle between the shear force and the crack face. Under a uniaxial tension loading $\theta = 0$, Eq. (55) reduce to $S = [(1 - 2\nu)/(4G)]\cdot {K_1}^2$. The stress ratio R, i.e., the minimal stress over the maximum stress, $\sigma_{\min}/\sigma_{\max}$

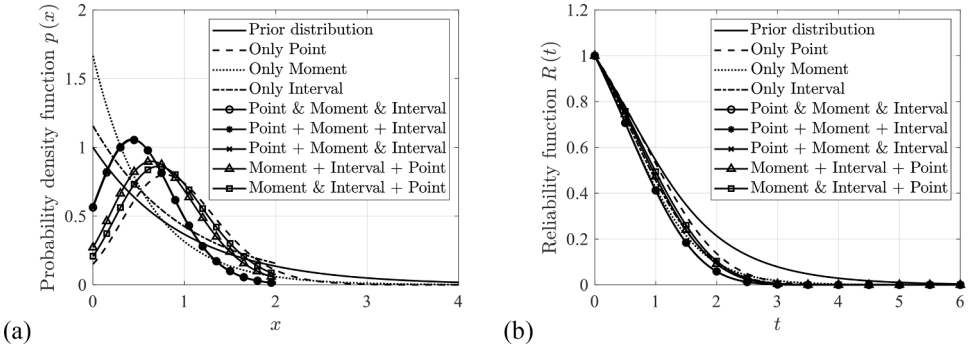

Fig. 3.. The comparisons between the prior and posterior distributions based on different information processing schemes. (a) Prior and posterior PDFs, and (b) reliability curves associated with the PDFs. The symbols "&" and "+" in the legends indicate simultaneous and sequential processing, respectively.

in one load cycle, can be incorporated through the function $U(R) = 0.55 + 0.33R + 0.12R^2$ [53]. In case of uniaxial loading with a stress ratio of R, the model simplifies to

$$\mathrm{d}a/\mathrm{d}N = B\left(\Delta S_{\mathrm{eff}}\right)^n = B\cdot\left\{(1-2\nu)/(4G)\cdot[U(R)\cdot\Delta K_I]^2\right\}^n, \tag{56}$$

where $\Delta K_I = g(a)\cdot\Delta\sigma\sqrt{\pi a}$, $\Delta\sigma = \sigma_{\max} - \sigma_{\min}$ is the stress variation in one load cycle, and $g(a)$ is the geometry factor associated with the geometry of the crack and specimen that can be found in, for example, Ref. [54].

Schijve et al. [53] reported the crack growth data of alloy D16 under different stress ratios, which are used for probabilistic information fusion combined with the strain energy density model. A set of specimens with a length of 500 mm, a width of 100 mm, and a thickness of 4 mm were fabricated, and a center through-thickness crack with an initial length of $a_0 = 5$ mm was prepared for each of the specimens. To demonstrate the information fusion process, the experimental data shown in Table 3 are grouped into four datasets according to the stress ratio R. The terms $\sigma_{\min}$, $\sigma_{\max}$, $\Delta\sigma$ are defined as before. The four datasets are obtained using specimens having the identical geometry and material configurations, but different loading parameters as identified by different σ_{min} and σ_{max} values. Dataset 1 is employed to estimate the mean value of parameters (B, n) in Eq. (56). Datasets 2 and 3 are used to obtain the moment information on (G, ν), representing an independent source of information in real cases. Dataset 4 is the validation set from which one data point of (a, N) is arbitrarily chosen to represent the actual measurement.

The material parameters (G, ν) and Young's modulus E relate to each other by $E = 2G(1 + \nu)$. Given the range of Young's modulus, a joint correlated interval constraint on (G, ν) is realized. As the material properties of alloy D16 are similar to that of the aluminum 2024-T3 alloy [53], the mean value of $(G, \nu) = (28.48,\ 0.34)$ associated with 2024-T3 given in Ref. [55] is used. A multivariate normal distribution is assumed for (G, ν) with a variation of coefficient of 0.1 and a coefficient of correlation of -0.1. In this case, the prior PDF for (G, ν) can be formed as a multivariate normal distribution with a mean vector of $[24.48, 0.34]$ and a variance-covariance matrix of $\begin{bmatrix} 8.111 & -0.009683 \\ -0.009683 & 0.001156 \end{bmatrix}$.

4.2.2. Updating with moment data

The combined fatigue crack growth testing data in Datasets 2 and 3 are used to obtain the representative moment information of (G, ν). The distribution of coefficient $a_{11} = (1-2\nu)/(4G)$ in Eq. (56) is obtained first with a mean vector and standard deviation of 3.5014×10^{-6} and 9.0207×10^{-8}, respectively. By incorporating the mean (0.3252) and standard deviation (1.084×10^{-2}) of the Poisson's ratio of aluminum 2024-T3 given in Ref. [56], the marginal samples of (G, ν) are used to obtain the moment data as

$$\begin{cases} \langle(G,\nu)\rangle = [24.9803 \quad 0.3252] \\ \langle\Sigma\rangle = \begin{bmatrix} 2.8117 & -1.6758\times10^{-2} \\ -1.6758\times10^{-2} & 1.1727\times10^{-4} \end{bmatrix}. \end{cases} \tag{57}$$

The posterior distribution obtained by probabilistic information fusion using the moment data, following Eq. (37), writes

$$p_m(G,\nu) = \exp\left\{-\frac{1}{2}\begin{bmatrix} G-28.48 \\ \nu-0.34 \end{bmatrix}^T \Sigma^{-1} \begin{bmatrix} G-28.48 \\ \nu-0.34 \end{bmatrix}\right\} \exp\left\{\beta_1 G + \beta_2 G^2 + \beta_3\nu + \beta_4\nu^2 + \beta_5 G\nu\right\} \tag{58}$$

The normalizing constant $Z_m = \int_\Theta p_m(G,\nu)\mathrm{d}G\mathrm{d}\nu$ and the coefficients $\beta_m = (\beta_1, \beta_2, \ldots, \beta_5)$ are determined by $\partial \ln Z_m/\partial(\beta_m) = \langle f(x)\rangle$ as $\beta_m = [167.45, -1.14, 26{,}933.02, -28{,}314.07, -341.67]$.

4.2.3. Updating with moment and correlated interval data

The interval of Young's modulus E can be transformed into the joint interval of parameter (G,ν), the variation intervals of shear modulus G and Young's modulus E are adopted as the interval data [55]. To demonstrate the interval effect, $G \in [22,\ 28]$ and $E = 2G\cdot(1+\nu) \in [55,\ 74]$ GPa are used as the correlated interval data. The results of the coefficients $\beta_i = (\beta_1, \beta_2, \ldots, \beta_5)$ are obtained as $\beta_i = [159.8970, -0.9858, 26{,}932.5481, -28{,}313.5953, -341.6670]$ with the moment and interval data.

4.2.4. Updating with point data

In addition to the updating with moment and interval data, the distribution is further updated with the point measurement data. This case represents the application where an initial PDF of the prediction model parameters is used, and some measurement data associated with the specific target are obtained to revise the PDF and prediction results. An arbitrarily chosen point from Dataset 4 is used as the measurement point $(N,\ a) = (60750,\ 11.6\ \mathrm{mm})$. The conditional probability for parameterized models based on the points observation is established as the likelihood function [57], the posterior distribution updated by the point measurement, following Eq. (51), is expressed as

$$p(G,\nu) \propto p_m(G,\nu) \times p(aG,\nu) = p_m(G,\nu) \times \frac{1}{\sqrt{2\pi\sigma_\epsilon^2}} \exp\left\{-\frac{[a - \mathscr{M}(G,\nu;N)]^2}{2\sigma_\epsilon^2}\right\}, \tag{59}$$

where $\mathscr{M}(G,\nu;N)$ is the crack length given the parameter of (G,ν) at cycle N and can be obtained by resolving the differential equation of Eq. (56) given the initial crack size $a_0 = 5$ mm.

4.2.5. Comparisons on the posteriors and probability of failures

In this study, the MCMC method with the standard Metropolis-Hasting algorithm [46] is employed to draw samples from the prior and resulting posterior PDFs. For each of the MCMC runs, a total number of 4×10^6 samples of (G,ν) are drawn. The samples associated with different PDFs are compared. Fatigue crack growth curves associated with different PDFs are obtained are obtained using the corresponding samples. The time-dependent reliability in terms of probability of failures (POFs) are evaluated with a failure criterion of $a_c = 10$ mm. Fig. 4 (a) and (b) present the comparisons on the prior and posterior PDFs of G and ν, respectively. Table 4 shows the corresponding mean vectors and variance-covariance matrices.

Based on the updated distributions of (G,ν) with different constraints, the comparisons on the fatigue crack growth prediction results of the validation set (Dataset 4) are made. The difference in crack growth prediction results is shown in Fig. 5(a). For example, the updated results with only moment information obtained using Datasets 2 and 3 outperform the prior results but still deviate from the actual testing result of Dataset 4. However, the prediction results updated with one measurement point from Dataset 4 can greatly improve the prediction performance. Results in Fig. 5(b) signify the influence of interval information on estimation results. For example, given a required risk of 10^{-4}, the difference of the remaining useful life prediction between the ones with and without interval constraint is about 400 cycles in this case study.

Table 3.
Loading parameters of fatigue testing data reported in Ref. [53].

Dataset	$\sigma_{\min}$(MPa)	$\sigma_{\max}$(MPa)	$\Delta\sigma$(MPa)	$R = \frac{\sigma_{\min}}{\sigma_{\max}}$	Usage
1	−26.7	53.3	80	−0.5	Estimation of (B, n)
2	32	96	64	0.33	Moment of (G, ν)
3	105	140	35	0.75	
4	0	64	64	0	Point data & Prediction validation

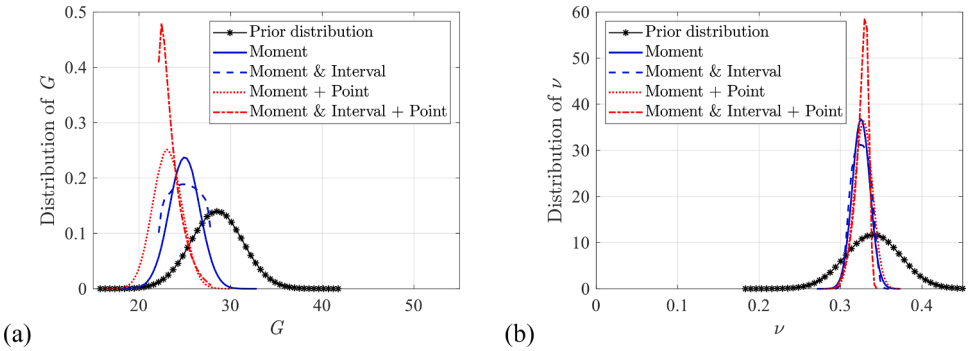

Fig. 4.. The prior and updated PDFs of the parameter. (a) G, and (b) ν.

Table 4.
Mean vectors and variance-covariance matrices of parameter $(\boldsymbol{G},\boldsymbol{\nu})$ associated with prior and posterior PDFs.

Constraints	Mean vector	Covariance matrix
Prior	[28.4697 0.3395]	$\begin{bmatrix} 8.1845 & -0.0098 \\ -0.0098 & 0.001134 \end{bmatrix}$
Moment	[25.0461 0.3248]	$\begin{bmatrix} 2.7677 & -0.01647 \\ -0.01647 & 0.0001535 \end{bmatrix}$
Moment & Interval	[24.9525 0.3253]	$\begin{bmatrix} 2.6125 & -0.01556 \\ -0.01556 & 0.0001011 \end{bmatrix}$
Moment + Point	[23.0997 0.3282]	$\begin{bmatrix} 2.4865 & -0.01661 \\ -0.01661 & 0.0001182 \end{bmatrix}$
Moment & Interval + Point	[23.4584 0.3258]	$\begin{bmatrix} 1.3442 & -0.008879 \\ -0.008879 & 6.5991\times10^{-5} \end{bmatrix}$

4.3. Lifing of turbine disk based on design target risk

A real risk-informed aeroengine part lifing in airworthiness is presented. An implicit interval information is incorporated using the proposed method. With this piece of information, the assessment is revised to produce a meaning result under the required risk level.

The prescribed safe life of turbine disk is the key to life management as noted in advisory documents of major airworthiness agencies, such as FAA [58] and EASA [59]. Apart from the numerical design validation, the spin rig test is required to determine the prescribed safe life for the safe operation of turbine engines. The spin rig test simulates the condition of the actual turbine disk in operation by applying appropriate rotational speed, acceleration and temperature. A fatigue load is formed in the startup-shutdown cycle of the spin. The startup-shutdown cycle is repeated until the disk fails. The number of samples is very small, usually less than 5, due to the cost and time [60]. Therefore, it is allowed to incrementally update this prescribed safe life when new test samples or service samples become available.

The statistical lifing method outlined in Ref. [61] is used to calculate the prescribed safe life. The basic assumption is that the actual life follows a log-normal distribution or Weibull distribution. In this study, the log-normal distribution is used and the log-transformed life follows a normal distribution with unknown mean (μ) and standard deviation (σ). To enable a risk-informed lifing result, it is necessary to estimate the unknown parameters (μ,σ) from the sparse samples. Without applying unvalidated opinions on the parameters, the noninformative prior for (μ,σ), Jeffreys' prior $p_0(\mu,\sigma)\propto 1/\sigma$, is used [62, 63]. The posterior PDF of (μ,σ) writes, according to Eq. (33), as

$$p(\mu,\sigma D)\propto 1/\sigma\cdot p(D\mu,\sigma), \tag{60}$$

where $p(D\mu,\sigma)$ is the conditional probability density function or the proportional likelihood, and D is the sample of log-lifetime. Based on the log-normal life distribution assumption,

$$p(D\mu,\sigma)=\prod_{i=1}^{k}\frac{1}{\left(\sqrt{2\pi}\,\sigma\right)^{k}}\exp\left[-\frac{(n_i-\mu)^2}{2\sigma^2}\right], \tag{61}$$

where $n_i, i=1,\ldots,k$ is the logarithm of the lifetime samples measured in cycles, and k is the total number of life samples.

4.3.1. Initial prescribed safe life

Three samples provided by a vendor are used for prescribed safe life determination and reliability assessment as shown in Table 5, where the numbers are actual number of cycles before failure. Taking logarithm to have the point data $D=(n_1,n_2,n_3)=(9.66,10.35,10.00)$.

A total number of 10^7 MCMC samples are drawn from the posterior PDF of Eq. (60), and results are shown in Fig. 6(a). The cumulative POF is obtained using MC estimator with the samples. For each of the MCMC samples, the cumulative POF associated with the sample is obtained using the cumulative distribution function. The failure rate or hazard rate function is obtained by

$$h(n)=-\frac{\mathrm{d}\ln R(n)}{\mathrm{d}n}=\frac{f(n)}{1-F(n)}, \tag{62}$$

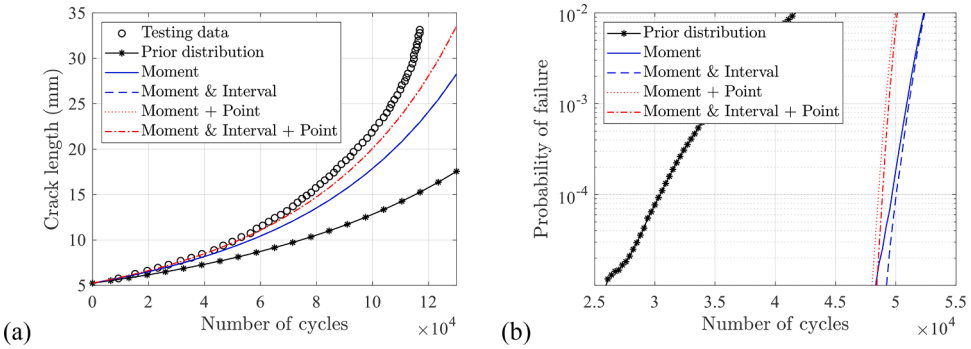

Fig. 5.. Comparison of the validation data set and the prediction results obtained with different information. The symbols "&" and "+" in the legends indicate simultaneous and sequential updating, respectively. (a) The crack growth, and (b) the time-dependent reliability.

where $R(n)$ is the reliability at cycle n, $f(n)$ and $F(n)$ are the PDF and CDF of the life evaluated at n, respectively, and $R(n) = 1 - F(n)$ by definition. Using the hazard rate function, the results of failure rate in terms of failure per hour is obtained using the MC estimator, and results are presented in Fig. 6(b) where an average exchange rate of 2.5 h/cycle is used to convert number of cycles to flight hours.

It is shown that for a given risk such as 10^{-3} failure per hour, the safe life is about 1000 flight hours. However, for parts that can generate hazardous engine effect, the required risk is $10^{-7} \sim 10^{-9}$ per flight hour [58]. Therefore, relying on the three samples without any further information cannot guarantee a required safety requirement.

4.3.2. Update with one additional life test sample

One additional life test sample, 33798, was acquired later, and the prescribed safety life can be updated with this data. Using Eq. (60) as the prior, the posterior reduces to a regular Bayesian posterior which reads,

$$p_1(\mu, \sigma n_4) = p(\mu, \sigma D)\cdot\frac{1}{\sqrt{2\pi}\sigma}\exp\left[-\frac{(n_4-\mu)^2}{2\sigma^2}\right], \tag{63}$$

where $p(\mu, \sigma D)$ is given by Eq. (60), and $n_4 = \ln(33798)$. The same MCMC sampling and MC evaluation procedure is performed. The results are shown in Fig. 7.

Based on the results shown in Fig. 7(c), the safe life at the failure rate of 10^{-3}/h increases to 3200 flight hours or so. Adding one additional test sample can revise the safe life under the given failure rate, but this result still does not assure any usefulness when the required risk level ($>10^{-7}$/h) is demanded.

4.3.3. Update with implicit interval data from vendor

It is noted that based on the statistical lifing method with sparse test samples, it is difficult to obtain a meaningful lifing result. The previous disk life management program based on a variety of disks [60] has shown that the lifetime sample dispersion, measured as the ratio of the maximum life over the minimum life is less than a factor of 10. Although there is no detailed survey on the actual lives of each of those disks, this piece of information is still highly important. This essentially setup the an implicit or vague bound for the parameter σ in above posterior. This type of interval data, however, cannot be easily fused in conventional interval analysis as there is no actual value of the minimum and maximum but only the ratio of the two.

The probabilistic information fusion of this type of information using the proposed method can be made in a way by applying a justified assumption in statistical hypothesis testing. In small sample a rare event is less likely to happen, and the sparse samples obtained are assumed to be in the range between -3σ and 3σ of the distribution centered around the mean value [64]. With this assumption, it is easy to convert the implicit interval data to a mathematical constraint

$$\sigma = \frac{1}{6}\ln\frac{N_{\max}}{N_{\min}}, \tag{64}$$

where $N_{\max}$ and $N_{\min}$ are the unknown maximum and minimum values in the samples, respectively. With the ratio of $N_{\max}/N_{\min} \leq 10$, the interval is determined as $0 < \sigma < 0.384$.

With the interval data, the posterior obtained using the proposed method yields a much more meaningful result as shown in Fig. 8. Based on the result shown in Fig. 8(c), the prescribed safe life at a risk level of 10^{-9} is about 5000 flight hours.

The actual disk lifing example demonstrates that by incorporating an implicit interval data using the proposed method, a meaningful result for critical part lifing in airworthiness evaluations can be achieved. It should be noted that as long as the information is relevant to the problem under consideration, the probabilistic fusion method can produce more relevant reliability assessment results.

Table 5.
Disk life samples obtained in a spin rig test.

No.	1	2	3
Cycles to failure	15,721	31,504	22,107

5. Conclusion

A general probabilistic information fusion framework was developed from the perspective of hazard rate dynamics in this study, allowing for assigning and updating probability with point, moment, and interval data in a formal way. In particular, the relative information entropy is formulated using the hazard rate function instead of the probability density function. The allows for recasting the information fusion problem into a dynamical equation where the relative information entropy is a general 'action', and different types of information are boundary conditions. Therefore, the information fusion process is to seek the least action by finding the optimal hazard rate function, which can subsequently be solved using Euler-Lagrange equation. The sequence of information processing resembles as applying different boundary conditions of the equation of motion. The interval data, both independent or correlated, can naturally be dealt with in this framework as regular boundary conditions. Based on the current results, the following conclusions are drawn.

1 The maximum relative entropy formulated using the hazard rate function, instead of probability density function, provides a novel perspective on information fusion and a mathematical link to information dynamics. Point, moment and interval data are treated uniformly as boundary conditions for the equation of motion of the hazard rate dynamics.
2 The proposed method provides a rational and universal alternative to existing methods for interval analysis in uncertainty quantification. It provides a viable means for information fusion with correlated interval data, which are less formally handled so far. In addition, it demonstrates the possibility to fuse implicit or vague interval data such as those expressed as ratios.
3 The point data are commutative in terms of information fusion, and moment and interval types of data are not commutative. It is up to the practitioners how the available information should be used. The fusion mechanism shows that different orders of information fusion, simultaneously or sequentially, are different path constraints for the equation of motion of the hazard rate dynamics.
4 The engineering application examples in this study demonstrates that the interval information can make a difference in reliability assessment. The implicit interval shown in the aeroengine disk lifing signifies that for reliability assessment with unavoidable sparse samples, the fusion of relevant interval information can make a highly nontrivial difference in the result.

It is worth mentioning that the proposed framework provides a mathematical tool for probabilistic information fusion; however, the method itself does not justify whether the information being processed is correct or relevant to the problem being asked. The method does not deal with the amount and quality of the data being used. The arbitrariness in transforming the observed data into testable information, and the order in which the information is processed are independent of the method. Such a property is demonstrated in Section 4.1 where the same pieces of information were processed in different orders and the different results were obtained.

In addition, the point data in this framework is encoded as a Dirac delta function, representing a precise measurement. However, the actual measurement cannot be fully precise, the incorporation of point data as a distribution function or an interval centered on the nominal value will change the form of Eq. (3), and consequently alters the final results. This involves a further detailed derivation of the related equations, and will

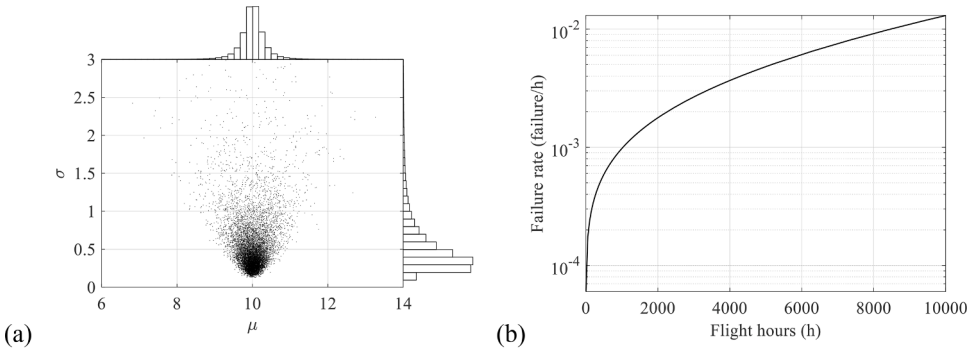

23

Fig. 6.. (a) The initial distribution of (μ, σ) estimated using three life test samples, and (b) the resulting failure rate with an exchange rate of 2.5 h/cycle.

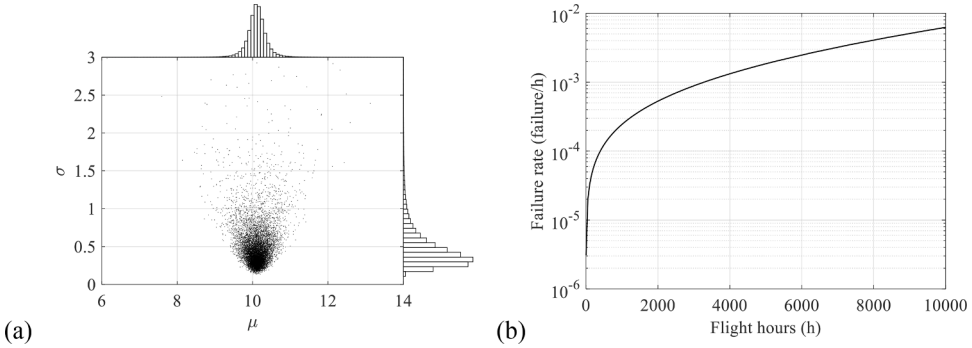

Fig. 7.. (a) The updated distribution of (μ, σ) using one additional life test sample, and (b) the resulting failure rate with an exchange rate of 2.5 h/cycle.

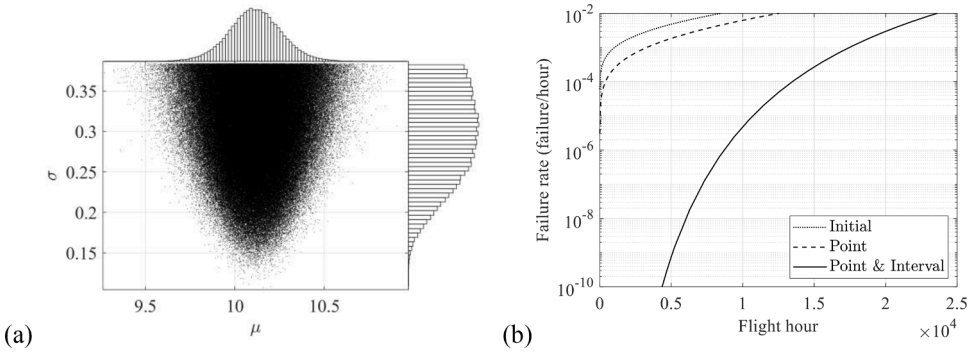

Fig. 8.. (a) The updated distribution of (μ, σ) using additional implicit interval data, and (b) comparisons of the failure rates with an exchange rate of 2.5 h/cycle.

be investigated in the future. The application of the developed method to more complex high-dimensional problems will also be pursued in the future work.

CRediT authorship contribution statement

Daoqing Zhou: Methodology, Writing - original draft. **Jingjing He:** Conceptualization, Methodology. **Yi-Mu Du:** Methodology, Formal analysis, Validation. **C.P. Sun:** Writing - review & editing. **Xuefei Guan:** Conceptualization, Methodology, Writing - review & editing.

Declaration of Competing Interest

The authors declare that they have no known competing financial interests or personal relationships that could have appeared to influence the work reported in this paper.

Acknowledgment

The study was supported by National Natural Science Foundation of China, Nos. 51975546, 11872088, U1930403 and by CAEP CX20200035. The support is gratefully acknowledged. Authors would like to thank the anonymous reviewers for their constructive comments.

Appendix

Applying the chain rule to the left hand side of EQ. (18) yields,

$$\begin{aligned}
&\frac{\partial \mathscr{L}}{\partial Y} - \sum_{i\in(x,t)} \partial_i \frac{\partial \mathscr{L}}{\partial[\partial_i Y]} + \partial_x\partial_t \frac{\partial \mathscr{L}}{\partial[\partial_x\partial_t Y]} \\
&= \&\frac{\partial \mathscr{L}}{\partial p}\frac{\partial p}{\partial Y} - \sum \partial_i\left(\frac{\partial \mathscr{L}}{\partial p}\frac{\partial p}{\partial[\partial_i Y]}\right) + \partial_x\partial_t\left(\frac{\partial \mathscr{L}}{\partial p}\frac{\partial p}{\partial[\partial_x\partial_t Y]}\right) \\
&= \& - \sum_i \left(\partial_i \frac{\partial \mathscr{L}}{\partial p}\right)\frac{\partial p}{\partial[\partial_i Y]} + \left(\partial_x\partial_t \frac{\partial \mathscr{L}}{\partial p}\right)\frac{\partial p}{\partial[\partial_x\partial_t Y]} \\
&+ \left(\partial_x \frac{\partial \mathscr{L}}{\partial p}\right)\left(\partial_t \frac{\partial p}{\partial[\partial_x\partial_t Y]}\right) + \left(\partial_t \frac{\partial \mathscr{L}}{\partial p}\right)\left(\partial_x \frac{\partial p}{\partial[\partial_x\partial_t Y]}\right) \\
&= \&\left(\partial_x\partial_t \frac{\partial \mathscr{L}}{\partial p}\right)\frac{\partial p}{\partial[\partial_x\partial_t Y]}.
\end{aligned} \tag{65}$$

The optimal solution is found by

$$\left(\partial_x\partial_t \frac{\partial \mathscr{L}}{\partial p}\right)\frac{\partial p}{\partial[\partial_x\partial_t Y]} = 0. \tag{66}$$

Note that $\frac{\partial p}{\partial[\partial_x\partial_t Y]} = -\exp(-Y) < 0$, indicating $\partial_x\partial_t \frac{\partial \mathscr{L}}{\partial p} = 0$. Expand the term to have

$$\partial_x\partial_t \frac{\partial \mathscr{L}}{\partial p} = \partial_x\partial_t\left[-\ln\frac{p}{p_0} - 1 + g\right] = -\partial_x\partial_t \ln\frac{p}{p_0} + \partial_x\partial_t g = 0 \tag{67}$$

Therefore,

$$\partial_x\partial_t\left[\ln\frac{p}{p_0}\right] = \partial_x\partial_t[g]. \tag{68}$$

Note that in Eqs. (65)-(68) the variable (x,t) in $p(x,t)$, $Y(x,t)$ and $g(x,t)$ are omitted and use short notations for simplicity. The general solution to Eq. (68) can be found as

$$\ln\frac{p(x,t)}{p_0(x,t)} = -a(x) - b(t) - c. \tag{69}$$

Reference

[1] Zhu B, Frangopol DM. Reliability assessment of ship structures using Bayesian updating. Eng. Struct. 2013;56:1836–47.
[2] Xu H, Gardoni P. Conditional formulation for the calibration of multi-level random fields with incomplete data. Reliab. Eng. Syst. Saf. 2020;204:107121.
[3] Green PJ. Reversible jump Markov chain Monte Carlo computation and Bayesian model determination. Biometrika 1995;82:711–32.
[4] Brooks S. Markov chain Monte Carlo method and its application. J. R. Stat. Soc. 1998;47:69–100.
[5] He J, Huo H, Guan X, Yang J. A Lamb wave quantification model for inclined cracks with experimental validation. Chin. J. Aeronaut. 2021;34:601–11.
[6] Yang J, He J, Guan X, Wang D, Chen H, Zhang W, et al. A probabilistic crack size quantification method using in-situ Lamb wave test and Bayesian updating. Mech. Syst. Sig. Process. 2016;78:118–33.
[7] Huo H, He J, Guan X. A Bayesian fusion method for composite damage identification using Lamb wave. Struct. Health Monitor. 2020:1475921720945000.
[8] Hossain NUI, Nur F, Hosseini S, Jaradat R, Marufuzzaman M, Puryear SM. A Bayesian network based approach for modeling and assessing resilience: a case study of a full service deep water port. Reliab. Eng. Syst. Saf. 2019;189:378–96.
[9] De Iuliis M, Kammouh O, Cimellaro GP, Tesfamariam S. Quantifying restoration time of power and telecommunication lifelines after earthquakes using Bayesian belief network model. Reliab. Eng. Syst. Saf. 2020:107320.
[10] Zhang Y, Weng W. Bayesian network model for buried gas pipeline failure analysis caused by corrosion and external interference. Reliab. Eng. Syst. Saf. 2020;203:107089.
[11] Choe D-E, Gardoni P, Rosowsky D. Closed-form fragility estimates, parameter sensitivity, and Bayesian updating for RC columns. J. Eng. Mech. 2007;133:833–43.
[12] Zhou Y, Li C, Zhou C, Luo H. Using Bayesian network for safety risk analysis of diaphragm wall deflection based on field data. Reliab. Eng. Syst. Saf. 2018;180:152–67.
[13] Choi W, Youn BD, Oh H, Kim NH. A Bayesian approach for a damage growth model using sporadically measured and heterogeneous on-site data from a steam turbine. Reliab. Eng. Syst. Saf. 2019;184:137–50.
[14] Sýkora M, Markova J, Diamantidis D. Bayesian network application for the risk assessment of existing energy production units. Reliab. Eng. Syst. Saf. 2018;169:312–20.
[15] Li C, Mahadevan S. Efficient approximate inference in Bayesian networks with continuous variables. Reliab. Eng. Syst. Saf. 2018;169:269–80.
[16] VanDerHorn E, Mahadevan S. Bayesian model updating with summarized statistical and reliability data. Reliab. Eng. Syst. Saf. 2018;172:12–24.
[17] Jaynes ET. Prior probabilities. IEEE Trans. Syst. Sci. Cybern. 1968;4:227–41.
[18] Jaynes ET. On the rationale of maximum-entropy methods. Proc. IEEE 1982;70:939–52.
[19] Shannon CE. A mathematical theory of communication. Bell Syst. Tech. J. 1948;27:379–423.
[20] Skilling J. Maximum Entropy and Bayesian methods: Cambridge, England, 36. Springer Science & Business Media; 2013. 1988.
[21] Du Y-M, Ma Y-H, Wei Y-F, Guan X, Sun C. Maximum entropy approach to reliability. Phys. Rev. E 2020;101:012106.
[22] Du Y-M, Chen J-F, Guan X, Sun C. Maximum entropy approach to reliability of multi-component systems with non-repairable or repairable components. Entropy 2021;23:348.
[23] Shore J, Johnson R. Axiomatic derivation of the principle of maximum entropy and the principle of minimum cross-entropy. IEEE Trans. Inf. Theory 1980;26:26–37.
[24] Caticha A, Giffin A. Updating probabilities. In: AIP Conference Proceedings; 2006. p. 31–42.
[25] Giffin A. From physics to economics: an econometric example using maximum relative entropy. Physica A 2009;388:1610–20.
[26] Guan X, Giffin A, Jha R, Liu Y. Maximum relative entropy-based probabilistic inference in fatigue crack damage prognostics. Probab. Eng. Mech. 2012;29:157–66.
[27] Arthern RJ. Exploring the use of transformation group priors and the method of maximum relative entropy for Bayesian glaciological inversions. J. Glaciol. 2015;61:947–62.
[28] Muñoz-Cobo J-L, Mendizábal R, Miquel A, Berna C, Escrivá A. Use of the principles of maximum entropy and maximum relative entropy for the determination of uncertain parameter distributions in engineering applications. Entropy 2017;19:486.
[29] Giffin A, Cafaro C, Ali SA. Application of the maximum relative entropy method to the physics of ferromagnetic materials. Physica A 2016;455:11–26.

[30] Xiao F. GIQ: a generalized intelligent quality-based approach for fusing multi-source information. IEEE Trans. Fuzzy Syst. 2020.
[31] Xiao F. Evidence combination based on prospect theory for multi-sensor data fusion. ISA Trans. 2020;106:253–61.
[32] Xiao F, Cao Z, Jolfaei A. A novel conflict measurement in decision-making and its application in fault diagnosis. IEEE Trans. Fuzzy Syst. 2020;29:186–97.
[33] Moore RE. Interval Analysis, 4. Prentice-Hall Englewood Cliffs; 1966.
[34] Wang X, Yang H, Qiu Z. Interval analysis method for damage identification of structures. AIAA J. 2010;48:1108–16.
[35] Yao R, Zhu W, Huang P. Accuracy analysis of Stewart platform based on interval analysis method. Chin. J. Mech. Eng. 2013;26:29–34.
[36] Gabriele S, Valente C, Brancaleoni F. An interval uncertainty based method for damage identification. Key Eng. Mater. 2007:551–6.
[37] Qiu Z, Wang X. Comparison of dynamic response of structures with uncertain-but-bounded parameters using non-probabilistic interval analysis method and probabilistic approach. Int. J. Solids Struct. 2003;40:5423–39.
[38] Rao SS, Berke L. Analysis of uncertain structural systems using interval analysis. AIAA J. 1997;35:727–35.
[39] Chen L, Rao SS. Fuzzy finite-element approach for the vibration analysis of imprecisely-defined systems. Finite Elem. Anal. Des. 1997;27:69–83.
[40] Qiu Z, Elishakoff I. Antioptimization of structures with large uncertain-but-non-random parameters via interval analysis. Comput. Meth. Appl. Mech. Eng. 1998; 152:361–72.
[41] McWilliam S. Anti-optimisation of uncertain structures using interval analysis. Comput. Struct. 2001;79:421–30.
[42] Qiu Z, Chen S, Song D. The displacement bound estimation for structures with an interval description of uncertain parameters. Commun. Numer. Methods Eng. 1996;12:1–11.
[43] Giffin A. Maximum Entropy: The Universal Method For Inference. 2009. arXiv preprint arXiv:0901.2987.
[44] Guan X, Jha R, Liu Y. Probabilistic fatigue damage prognosis using maximum entropy approach. J. Intell. Manuf. 2012;23:163–71.
[45] Wang Y, Liu Y. Bayesian entropy network for fusion of different types of information. Reliab. Eng. Syst. Saf. 2020;195:106747.
[46] Hastings WK. Monte Carlo Sampling Methods Using Markov Chains and Their Applications. 1970.
[47] Gregory P. Bayesian Logical Data Analysis for the Physical Sciences: a Comparative Approach With Mathematica® Support. Cambridge University Press; 2005.
[48] Guan X, He J, Jha R, Liu Y. An efficient analytical Bayesian method for reliability and system response updating based on Laplace and inverse first-order reliability computations. Reliab. Eng. Syst. Saf. 2012;97:1–13.
[49] He J, Guan X, Jha R. Improve the accuracy of asymptotic approximation in reliability problems involving multimodal distributions. IEEE Trans. Reliab. 2016; 65:1724–36.
[50] He J, Chen J, Guan X. Lifetime distribution selection for complete and censored multi-level testing data and its influence on probability of failure estimates. Struct. Multidiscip. Optim. 2020;62:1–17.
[51] Sih GC. Strain-energy-density factor applied to mixed mode crack problems. Int. J. Fract. 1974;10:305–21.
[52] Irwin GR. Crack-Extension Force for A Part-Through Crack in a Plate. 1962.
[53] Schijve J, Skorupa M, Skorupa A, Machniewicz T, Gruszczynski P. Fatigue crack growth in the aluminium alloy D16 under constant and variable amplitude loading. Int. J. Fatigue 2004;26:1–15.
[54] Tada H, Paris P, Irwin G. The Analysis of Cracks Handbook, 2. New York: ASME Press; 2000. p. 1.
[55] Tang CY, Lee WB. Effects of damage on the shear modulus of aluminum alloy 2024T3. Scr. Metall. Mater. 1995;32:1993–9.
[56] Alexopoulos ND, Dalakouras CJ, Skarvelis P, Kourkoulis SK. Accelerated corrosion exposure in ultra thin sheets of 2024 aircraft aluminium alloy for GLARE applications. Corros. Sci. 2012;55:289–300.
[57] Guan X, Jha R, Liu Y. Model selection, updating, and averaging for probabilistic fatigue damage prognosis. Struct. Saf. 2011;33:242–9.
[58] Administration Federal Aviation. AC 33.14-1 - Damage Tolerance for high energy turbine engine rotors. 2001.
[59] European Aviation Safety Agency. Acceptable Means of Compliance for Engines (CS-E). 2010. Amendment 3.
[60] Boyd-Lee A, Harrison G. The development of life extension methods for fracture critical aero-engine components. In: RTO Meeting proceedings; 1999. p. 18.1–8. .10.
[61] Standard 00-970 Part 1 Section 7 Design & Airworthiness Requirements For Service Aircraft. UK Ministry of Defense; 2003.
[62] Jeffreys H. The Theory Of Probability. Oxford: OUP; 1998.
[63] Guan X, He J. Life time extension of turbine rotating components under risk constraints: a state-of-the-art review and case study. Int. J. Fatigue 2019;129: 104799.
[64] Boyd-Lee A, Harrison G, Henderson M. Evaluation of standard life assessment procedures and life extension methodologies for fracture-critical components. Int. J. Fatigue 2001;23:11–9.